공학석사학위논문

Development of Pd-In/HCS Catalyst for Treatment of Nitrate and Nitrite in Drinking Water

먹는 물 중 질산염 및 아질산염 처리를 위한
Pd-In/HCS 촉매 개발

2019년 8월

서울대학교 대학원

건설환경공학부

홍 기 헌

Development of Pd-In/HCS Catalyst for Treatment of Nitrate and Nitrite in Drinking Water

먹는 물 중 질산염 및 아질산염 처리를 위한 Pd-In/HCS 촉매 개발

지도교수 최 정 권

이 논문을 공학석사 학위논문으로 제출함

2019년 8월

서울대학교 대학원
건설환경공학부
홍 기 헌

홍기헌의 석사 학위논문을 인준함
2019년 7월

위 원 장	한 무 영	(인)
부위원장	최 정 권	(인)
위 원	남 경 필	(인)

Abstract

Groundwater and surface water contamination with nitrate and nitrite keeps increasing all around the world due to the excessive use of fertilizer. Without the proper treatment, these contaminants can induce the blue baby syndrome(methemoglo-binemia) and cancer. Due to the harmful effect of these contaminants, the U.S. EPA has set the federal regulation on the maximum level of nitrate and nitrite in drinking water to be $10\ mg-N/L$ and $1\ mg-N/L$, respectively. Catalytic treatment is a promising technology that can sustainably reduce nitrate and nitrite to nitrogen gas using hydrogen as an electron donor. However, current research on the catalytic reduction has a limitation because of the production of ammonia as a by-product. In this study, we have developed Hollow Carbon Sphere(HCS) supported Pd-based catalysts, which yields very low concentration of ammonia during nitrite reduction. To further investigate the physicochemical characteristics of the Pd and Pd-In/HCS catalyst, we have conducted various analysis such as morphology of catalyst, metal dispersion,

crystalline structure, and chemical state of noble metals by using transmission electron microscopy, X-ray diffraction, and X-ray photoelectron spectroscopy. The role of the noble metal and HCS on the reaction pathway of reduction of nitrate to nitrogen over ammonia was further examined by evaluating the crystalline structure and chemical state of Pd and In bimetallic catalysts. Findings from this study has a broader implication to improve the selectivity of catalysts and minimize the formation of undesired by-product during nitrate treatment.

Keyword : Nitrate and nitrite removal; Catalytic reduction; Pd-In Catalyst; Groundwater; Ammonia
Student Number : 2017-20809

Table of Contents

Contents of Table

Contents of Figure

Chapter 1. Introduction

1.1 Background

Nitrate (NO_3^-) contamination which is commonly results from overuse of agricultural fertilizers, sewage discharges, and contaminant leachate from landfills. This contaminant is one of the common contaminant detected from groundwater and surface water.[1] Nitrate contamination of drinking water is the greatest public health threats around the world.[2] Drinking nitrate contaminated water raises serious human health problem, such as blue baby syndrome(methemoglobinemia), cancer, and hypertension, since nitrate can be transformed into nitrite (NO_2^-) and/or N-nitroso compounds.[3-5] Because of these risks, the United States Environmental Protection Agency (USEPA) limits the maximum contaminant levels(MCL) of nitrate and nitrate to $10\,mg-N/L$ and $1.0\,mg-N/L$, respectively.[6]

Several technologies are widely used to remove nitrate and

nitrite in drinking water, including ion exhchange[7,8], reverse osmosis[9], electrodialysis[10], biological denitrification[11,12]. These technologies have demonstrated their effectiveness in large or small scale treatment.[13,14] However, the principal drawback of ion exchange, reverse osmosis, electrodialysis is that these treatments produce concentrated nitrate and nitrite brine which must be further treated prior to disposal.[15–20] Unlike the previous technologies, the biological denitrification process is being used more widely in the field of municipal and industrial wastewater. However, a risk of pathogen introduction and biological sludge generation have limited their application for drinking water treatment.[15,16] More recently, catalytic reduction of nitrate and nitrite with noble metal based bimetallic catalyst has emerged as a promising technology not only because of the simple procedure of the catalysis but also because of the high selectivity to nitrogen gas($N_{2(g)}$) over harmful ammonia (NH_3).[19,20] Among various noble metal, palladium (Pd) has been reported as the most effective metal for rapid reduction of nitrate to nitrogen gas using hydrogen gas as a reducing agent

when present with secondary promoter metal such as indium, copper, tin, and nickel.[21–23] So far, studies on the catalytic role of Pd have shown that Pd alone cannot remove nitrate.[1,17,24–28] Instead, promoter metal such as In and Cu is used to reduce nitrate to nitrite, and the reduced nitrite is transferred to adjacent Pd surface and is further reduced to nitrogen gas or ammonia using hydrogen dissociated from hydrogen gas at the surface of Pd.[26,27,29] In particular, it is known that Pd and In bimetallic catalyst is capable of very high activity and selective reduction of nitrate to nitrogen.[30–32]

Mechanistically, nitrate is first reduced to nitrite on the surface of metallic In that oxidizes. In this process, fortunately, hydrogen adatoms adsorbed on Pd spillovers to In oxides that eventually reduces to metallic In. Thus, nitrate can be continuously reduced to nitrite only on the promoter metal, In. The nitrite then transfers to neighboring Pd surface to be further reduced to nitrogen gas or ammonia using hydrogen adatoms. There are research results focusing on the metal loading, metal nanoparticle size, atomic configuration, type of promoter metal in the case of reduction rate and selectivity.[33–36]

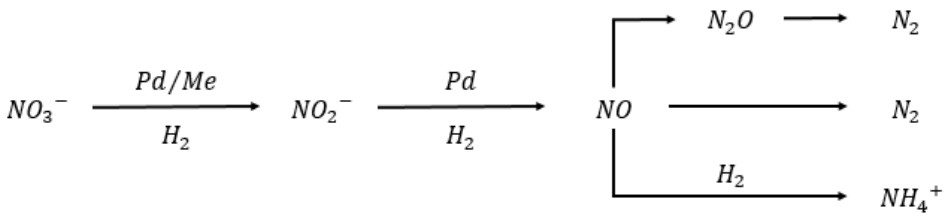

Figure 1 Schematic diagram of the catalytic nitrate reduction

As part of the Pd-based catalyst, I. Stolarov et al. found the unsupported heterobimetallic acetate-bridged complexes $Pt^{II}(\mu - OOCMe)_4M^{II}(HOOCMe)_4\ (M = Ca, Sr, Ba)$ efficiently catalyze partial alkyne hydrogenation in the liquid phase[46] and N. Kozitsyna et al. developed a similar catalytic effect for the synthesis of Pd-based analogous $Pd^{II}(\mu - OOCMe)_4M^{II}(HOOCMe)_4\ (M = Ca, Sr, Ba)$.[47] Recently, developing Pd-based heterobimetallic complex with group 13 elements such as Ga, In, Tl has been attempted.[48–50] Since Palladium(II)-Indium(II) acetate bridged complex consists of palladium and indium next to each other, this heterometallic catalyst was intended to made for rapid reduction of nitrate.

Up to now, a great effort has been devoted to the design and manufacture of nanostructured composites for potential applications in heterogeneous catalysts.[37,38] Deposition of noble

metal nanoparticles onto the surface of inorganic or polymeric microspheres has been paid particular attention due to its ability to prevent aggregation of noble metal nanoparticles which ensures the catalytic activity in heterogeneous catalysis.[39] Especially hollow carbon spheres (HCSs) have been in focus of study by both academy and industry due to its unique structure and potential application in numerous field including catalysis as a support material, which enrich the already broad family of carbon materials. One of the obvious way to make HCSs with uniform structure is to carbonize core–shell polymer particles.[40] The main advantage of this method is that it can remove the polymer core and form a carbon shell concurrently without any additional core etching process. By controlling the decomposition temperature of the two polymers, in which the core polymer has a low decomposition temperature and the shell polymer has a high decomposition temperature, HCSs can be uniformly formed by removing the core polymer and carbonizing the shell polymer as carbon. Overall procedure to make HCS is shown in Figure 2.

There were several studies on selection of organic

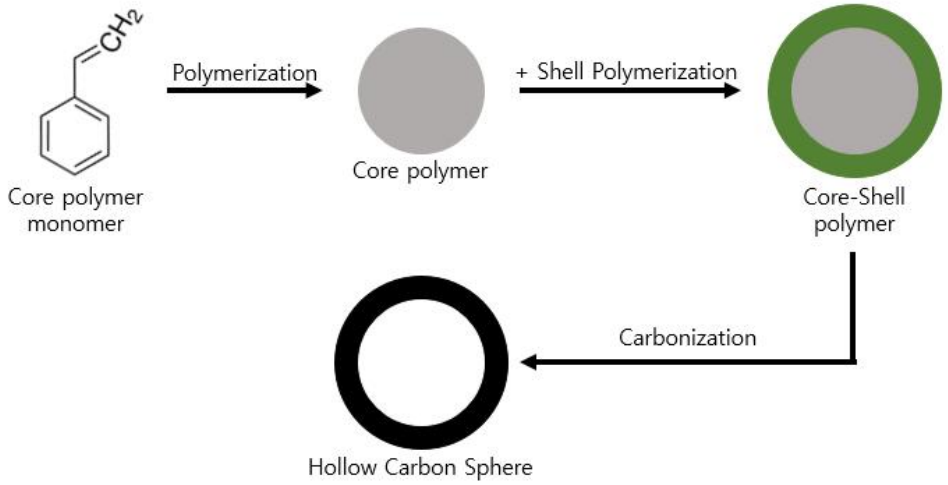

Figure 2 Schematic illustration of the synthesizing HCSs

polymers for core and shell template. For core polymers, polystyrene (PS), polyethylene, polymethyl methacrylate, and for shell polymers, polyacrylonitrile, polydivinylbenzene, phenol-formaldehyde resin, poly furfuryl alcohol.[40-43] Theoretically, there can be variety of combinations for these two kinds of polymers. Although there have been several attempts to carbonize different core-shell polymers such as PMMA/PAN[40], PS/PAN[41], PS/PF[42], and PMMA/PDVB[43], X. Y. Dai et al[44] reported one-step carbonization of PS/PANi core-shell polymer spheres in a simple and effective way to form HCS within a good hollow spherical shape.

1.2 Objectives

In this study, combined with Pd and In metal precursor and hollow carbon sphere, Pd-In bimetallic catalysts (Pd-In/HCS) were prepared by the incipient wetness impregnation method followed by the atmospheric phase reduction using hydrogen gas and then applied in the liquid phase catalytic reduction of nitrate and nitrite. Four different catalysts were synthesized and their catalytic activity and selectivity influenced by the catalyst, different calcination and reduction temperatures, and the metal precursor (metal salt as conventional method and Pd-In complex) are also discussed in detail with physicochemical characterizations by transmission electron microscopy(TEM), X-ray diffraction(XRD), and X-ray photoelectron spectroscopy(XPS). Therefore, the objectives of this study are to develop Pd and Pd-In catalysts supported on hollow carbon sphere(HCS), to investigate the physicochemical characteristics of the Pd and Pd-In/HCS catalyst, and to quantify catalysts reactivity for the NO_3^- and NO_2^- reduction.

Chapter 2. Materials and Methods

2.1 Materials

All reagents used in this study were purchased from Alfa-Aesar, Sigma Aldrich, and Korea Special Gas. The chemicals were used without further purification unless otherwise stated, and listed as below;

- Alfa Aesar :

Styrene (St, extra pure, 99%), $In(OAc)_3$ (99.99%), diethyl ether (99+%), D(+)-glucose, citric acid monohydrate, trisodium citrate dihydrate,

- Sigma Aldrich :

azobisisobutyronitrile (AIBN, 12wt% in acetone), poly(vinylpyrrolidine) (PVP, K-30), Isopropanol (70% in H_2O), ammonium persulfate (ACS reagent, 98+%), aniline (≥

99.5%), $Pd(NO_3)_2 \cdot 2H_2O$, $Pd(OAc)_2$, $In(NO_3)_3 \cdot xH_2O$, sodium dodecyl sulfate, methanol (99.99%), ethanol (95%), palladium nitrate dihydrate $(\mathrm{Pd}(NO_3)_2 \cdot 2H_2O)$, indium nitrate hydrate $(\mathrm{In}(NO_3)_3 \cdot xH_2O)$.

– Korean Special Gas :

H2 gas(99.999%), N2 gas(99.999%)

Distilled water (DIW) was treated by N2 bubbling for 30 min before use. The simulated nitrate and nitrite stock solution was prepared by dissolving certain amount of $NaNO_2$ or $NaNO_3$ in DIW to set 15 mM which would be injected into the reactor to make 1 mM of initial concentration.

2.2 Methods

2.2.1 Support Material

2.2.1.1 Synthesis of polystyrene (PS) microspheres

Poly(N-vinylpyrrolidone) (PVP)-stabilized polystyrene-(PS) microspheres were synthesized without any surface pretreatments according to the previously reported method by Armes et al[45]. Azobisisobutyro-nitrile (AIBN) was distilled under vacuum and recrystallized before being used. 2.8 g of PVP dissolved in 160 mL of isopropanol was added to 250 mL of three-neck round bottom flask. The solution was then heated up to 70℃ and simultaneously bubbled with $N_{2(g)}$ for the purpose of removing any dissolved oxygen which is an inhibitor for the synthesis under stirring at 500 rpm. 0.2 g of AIBN predissolved in 23 mL of styrene was then injected to the

reactor under vigorous stirring at 900 rpm to initiate the polymerization. After 24 hours of reaction, the reactor was cooled down to room temperature, The PS particles were separated with solution by 3 cycles of centrifuge(13500g)/wash/redisperse in DIW and dried in 65℃ oven overnight.

2.2.1.2 Preparation of Polystyrene/Polyaniline (Ps/PANi) core-shell polymer and HCS

Above dried PS particles (5 g) were dispersed in 500 mL of DIW and maintain at 0 ℃ under stirring (500 rpm). Subsequently, 3 mL of aniline was dissolved in 66 mL of HCl (2M) and 7.5 g of ammonium persulfate was dissolved in 30 mL of DIW. Aniline solution and ammonium persulfate solution was then cooled down to 0℃. Aniline solution was then added to the PS dispersed solution with stirring at 0℃ for at least 5 hours followed by slowly dropping ammonium persulfate solution into the above mixture for 18 hours to initiate polymerization.

Obtained PS/PANi core-shell product in the solution was then settled down and the supernatant was substituted with DIW by 3 cycles, then removed the supernatant as much as possible. Remaining solution was then delivered to the 65℃ oven and dried overnight. Dried PS/PANi core-shell particles was drenched with methanol and let it dried with a little manual stirring not to aggregate themselves. The obtained PS/PANi core-shell particles was put into a tubular furnace. Firstly, heated up to 450℃ at a rate of $1\,℃/min$ and held for 30 min to completely eliminate PS core, and then immediately heated up to 800℃ at a rate of $2\,℃/min$ and held for 180 min to change PANi shells into carbon shells.

2.2.2 Metal Precursor

2.2.2.1 Pd-In Acetate Bridged Complex (Pd-In Complex)

224 mg of palladium acetate (1 mmol based on Pd) and 292 mg of indium acetate (1mmol based on In) was mixed in 7 mL of glacial acetic acid under reflux and stirring (450 rpm) at 80℃. When the solution forms a clear yellow-orange solution, cool down to room temperature. A yellowish orange fine-crystalline was filtered off with diethyl ether and dried in a desiccator over silicagel.

2.2.2.2 Pd & In solutions

Aqueous solutions of corresponding metal precursor salts are prepared by dissolving palladium nitrate dihydrate ($\mathrm{Pd}(NO_3)_2 \cdot 2H_2O$) and indium nitrate hydrate ($\mathrm{In}(NO_3)_3 \cdot xH_2O$) into DIW without any further purification.

2.2.3 Catalysts Preparation

The Pd and Pd-In catalyst supported by HCS was prepared by the incipient wetness impregnation method. The metal loading on the support was 5wt% palladium and 2wt% indium from aqueous solutions of corresponding metal precursor salts, palladium nitrate dihydrate $(\mathrm{Pd}(NO_3)_2 \cdot 2H_2O)$ and indium nitrate hydrate $(\mathrm{In}(NO_3)_3 \cdot xH_2O)$. Also, 5wt% palladium and 5wt% indium were deposited onto the support by the incipient wetness impregnation method using Pd-In complex solution (the mixture of DIW and acetic acid, DIW : acetic acid = 1:3). After impregnation, the samples were calcined under nitrogen flow for 30 min and reduced under hydrogen flow for 2 h. Depending on the metal precursor used, different temperatures were selected for calcination and reduction. Using metal salt as precursor, Pd(5wt%)/HCS and Pd(5wt%)-In(2wt%)/HCS were calcined under nitrogen flow for 30 min at 120℃ and reduced under hydrogen flow for 2 h at 450℃. Another Pd(5wt%)-In(2wt%)/HCS were calcined under nitrogen flow for 4 h at

550℃ and reduced under hydrogen flow for 2 h at 450℃. Using metal complex as precursor, Pd(5wt%)-In(5wt%)/HCS were calcined under nitrogen flow for 30 min at 120℃ and reduced under hydrogen flow for 2 h at 120℃. Additionally, Pd(5wt%)-In(5wt%)/HCS was calcined under nitrogen flow for 4 h at 550℃ and reduced under hydrogen flow for 2 h at 450℃. All catalysts above are listed in Table 1. Numeric subscript denotes the metal loading and the subscripts in parentheses mean metal precursors (S : metal salt, C : Pd-In complex). For convenience, the numeric subscripts will be omitted from the name of each catalyst. The subscripts next to HCS in all catalysts will be used for indication of the reduction temperature.

Table 1 Catalyst preparation

Catalyst	Calcination Temp.	Reduction Temp.
$\boldsymbol{Pd_{5(S)}/HCS}$	120	450
$\boldsymbol{Pd_5 - In_{2(S)}/HCS}$	120 550	120 450
$\boldsymbol{Pd_5 - In_{5(C)}/HCS}$	120 550	120 450

2.2.4 Catalytic Reduction Experiments

The reduction of nitrate and nitrite was carried out in a semi open batch system under continuous $H_{2(g)}$ sparging $(1atm,\ 200\ mLmin^{-1})$ at constant temperature of 25℃. In a 250 mL of three-neck round bottom flask, 140 mL of buffer solution and predetermined mass of catalyst (0.03 g) was filled. The suspended solution was then sonicated for 10 min and $H_{2(g)}$ was sparged for 30 min before introducing 10 mL of nitrate or nitrite stock solution (15mM as NO_3^- or NO_2^-) to initiate the catalytic reduction of nitrate or nitrite. Reaction was monitored by periodic sampling (1 mL) from the reactor

that are immediately filtered by 0.22 μm polyethersulfone syringe filter to remove catalyst particles. The reaction was carried out by mixing with a Teflon-coated magnetic stir bar at 850 rpm. pH was maintained by 10 mM of pH 5 citric-citrate buffer solution. General operation condition of catalytic nitrate and nitrite reduction are summarized in Table 2.

Table 2 Operating conditions of catalytic reduction

Initial NO_3^- or NO_2^- concentration (mM)	1
Catalyst concentration (g/L)	0.2
Hydrogen gas flow rate (mL/min)	200
pH	5
Reaction Temparature (℃)	25
Operating Pressure (bar)	1

2.2.5 Determination of catalytic activity and selectivity

The catalytic activity for the reduction experiment of nitrate and nitrite was determined by the observed reaction rate constant assuming pseudo first-order dependence on nitrate and nitrite concentration as below,

$$-\frac{dC_{NO_x^-}}{dt} = kC_{NO_x^-}$$

where $C_{NO_x^-}$ and t is the concentration of nitrate or nitrite and time, respectively. The measured rate constants were calculated as Pd mass normalized pseudo-first-order rate constant for substantive comparison of catalytic activity, k_{norm} (with units of $L\,min^{-1}\,g_{pd}{}^{-1}$).

Previous studies have shown that a large amount of intermediate products, $NO_{(g)}$ and $N_2O_{(g)}$, are produced during nitrate and nitrite reduction.[30,31,51] Although some portions of $N_2O_{(g)}$ is formed as a transient intermediate in the reduction of nitrate and nitrite by Pd-based catalysts in the headspace, it

has been reported that $NO_{(g)}$ is not detected during the reduction of nitrate and nitrite.[51,52] Therefore, the selectivity to $N_{2(g)}$ (S_{N_2}), NH_4^+ ($S_{NH_4^+}$), and NO_2^- ($S_{NO_2^-}$) are calculated as follows:

$$S_{N_2} = 100 - S_{NH_4^+} - S_{NO_2^-}$$

$$S_{NH_4^+} = \left(\frac{C_{NH_4^+}}{C_0 - C}\right) \times 100$$

$$S_{NO_2^-} = \left(\frac{C_{NO_2^-}}{C_0 - C}\right) \times 100$$

where, C_0, C, $C_{NH_4^+}$, and $C_{NO_2^-}$ is initial nitrate or nitrite concentration, concentration after reaction, concentration of ammonia, and concentration of nitrite, respectively.

2.2.6 Catalytic Characterization

The catalysts were characterized by high resolution-transmission electron microscope (HR-TEM), transmission electron microscope II (ccd camera type), powder X-ray diffractometer (XRD), X-ray photoelectron spectroscopy (XPS), inductively coupled plasma - optical emission

spectrometry (ICP-OES), and inductively coupled plasma - mass spectrometry (ICP-MS). HR-TEM and TEM II was carried out on a JEM-3010 and JEM-2100, respectively. Samples for the analysis were dispersed in ethanol, sonicated, and deposited on a lacey formvar film stabilized with carbon grid. XRD spectra of catalysts were recorded in the range between $2\theta = 3 - 90^{\circ}$ by RigakuD/teX Ultra 250. XPS analysis was performed by Kratos AXIS-His with Mg/Al anode material. Metals deposited on the support material was analyzed with ICP-OES.

Chapter 3. Results and Discussion

3.1 Catalysts Characterization

3.1.1 TEM results

The TEM image of synthesized core polymer PS and core-shell polymer Ps/PANi is shown in Figure 3. Figure 3A and B represents the PS latex beads and Figure 3C and D represents the synthesized PS/PANi particles. The PS particle was found to have a uniform size distribution with an average diameter of 854 nm and had a smooth surface. PS particles were then coated with aniline monomers with assistance of ammonium persulfate to form core-shell polymer particle. As can be seen in TEM image of Figure 3C and D, it is clear that PS particle was coated with aniline polymer to form a shell outside of PS particle.

Figure 4 represents TEM images of the as obtained HCS

after carbonizing PS/PANi core-shell polymer. Figure 4A and B shows the overall morphology of HCS. After carbonization of PS/PANi, HCS was confirmed to have well-defined hollow structure since it can be easily seen to have different contrasts at outer part of HCS (darker shade) and inner part of HCS (whiter shade). Although hollow structure of HCS was clearly confirmed, aggregation of mono-dispersed HCS is also shown. This is probably due to the possibility that the aniline polymers are clustered in the process of polymerizing on the PS surface or, in the process of making PS, not all spheres are created independently, but are made up of one another. In the closer examination on these HCSs in Figure 4C and D, the HCS carbonized from PS / PANi had a rugged surface while the PS surface was smooth. This is probably due to the uneven adhesion of polymerized aniline on the PS surface. The average size of HCS was measured to be 895 nm with a carbon shell thickness of 90 nm and its distribution is shown in Figure 5A and B.

For catalytic reduction of nitrate and nitrite, Pd and In were deposited onto the support material, HCS. From Figure 6 to

Figure 10, TEM images of $Pd_{(S)}/HCS_{(450)}$, $Pd-In_{(S)}/HCS_{(120)}$, $Pd-In_{(S)}/HCS_{(450)}$, $Pd-In_{(C)}/HCS_{(120)}$, and $Pd-In_{(C)}/HCS_{(450)}$ are shown in order. Figure 6A and B is a TEM image of $Pd_{(S)}/HCS_{(450)}$ catalyst, and metal particles are very uniformly distributed on the surface. Most of the particles were in the range between 3 - 6 nm, and the average was 4.6 nm. $Pd-In_{(S)}/HCS_{(120)}$ and $Pd-In_{(S)}/HCS_{(450)}$ catalyst is shown in each Figure 7 and 8. It can be confirmed that the distribution of the metal is fine. However, the aggregation of metals was found in the latter catalyst in which the reducing temperature was increased. As it can be reconfirmed in the histogram from Figure 7 and 8, the increase in the particle size of the metal was resulted from the increase in reducing temperature. These results are in good agreement with those reported earlier.[53–55]

For heterometallic Pd–In acetate bridged complex as noble metal precursor, TEM analysis was conducted to investigate the morphological characteristics of $Pd-In_{(C)}/HCS_{(120)}$ and $Pd-In_{(C)}/HCS_{(450)}$ catalysts. It should be noted that the catalyst ($Pd-In_{(C)}/HCS_{(450)}$) reduced at 450℃ showed much higher

wide distribution of metal nanoparticles on the surface of the HCS as shown in Figure 10A and B rather than the catalyst ($Pd-In_{(C)}/HCS_{(120)}$) reduced at 120℃ as shown in Figure 9 where the metal nanoparticles were aggregated along themselves or even did not deposited. Most of the particles from $Pd-In_{(C)}/HCS_{(450)}$ catalyst were in the range between 6 – 10 nm, and the average diameter was 7.3 nm. These values are slightly higher than the catalyst made by the metal precursors as described earlier and are ascribe to the fact that the Pd and In metals are alloyed.

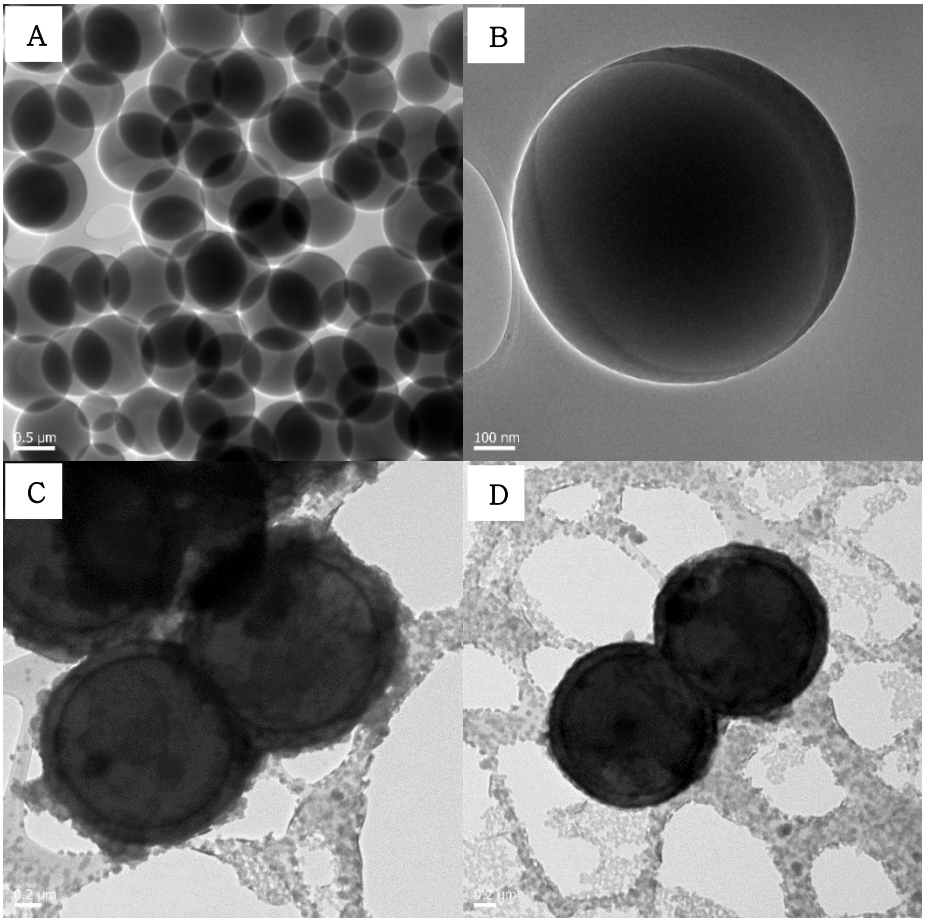

Figure 3 TEM images of PS (A, B) and PS/PANi (C,D)

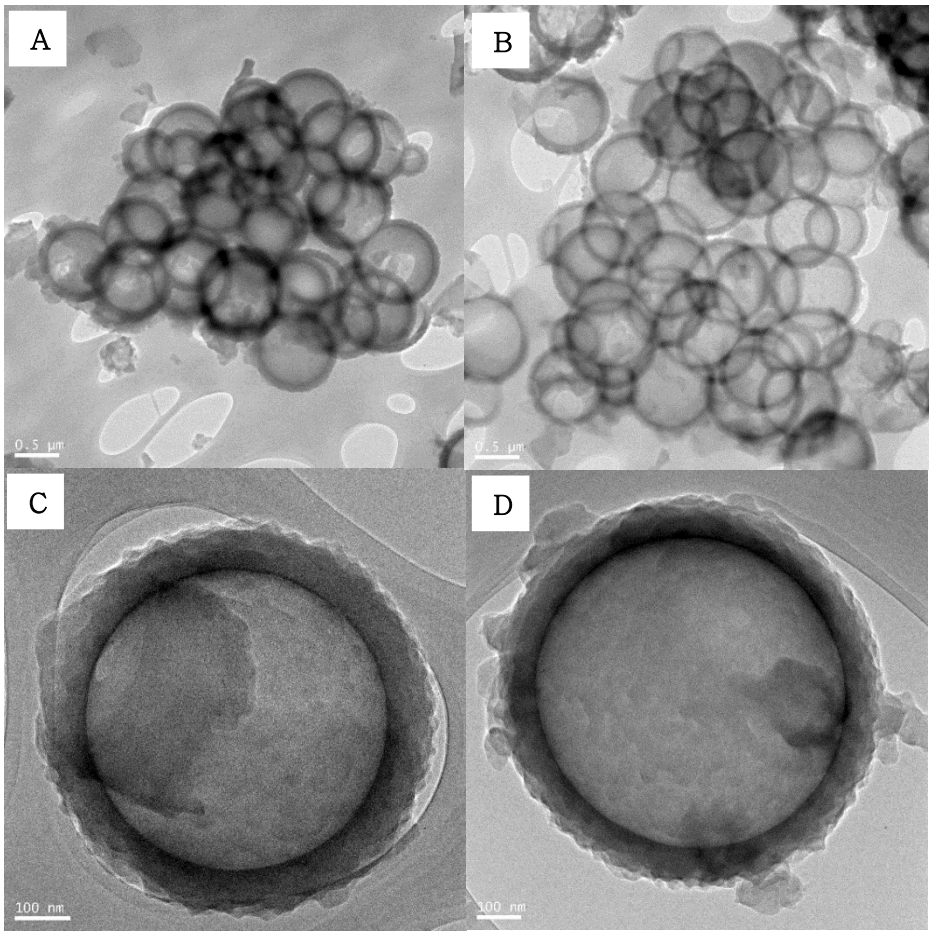

Figure 4 TEM images of HCS

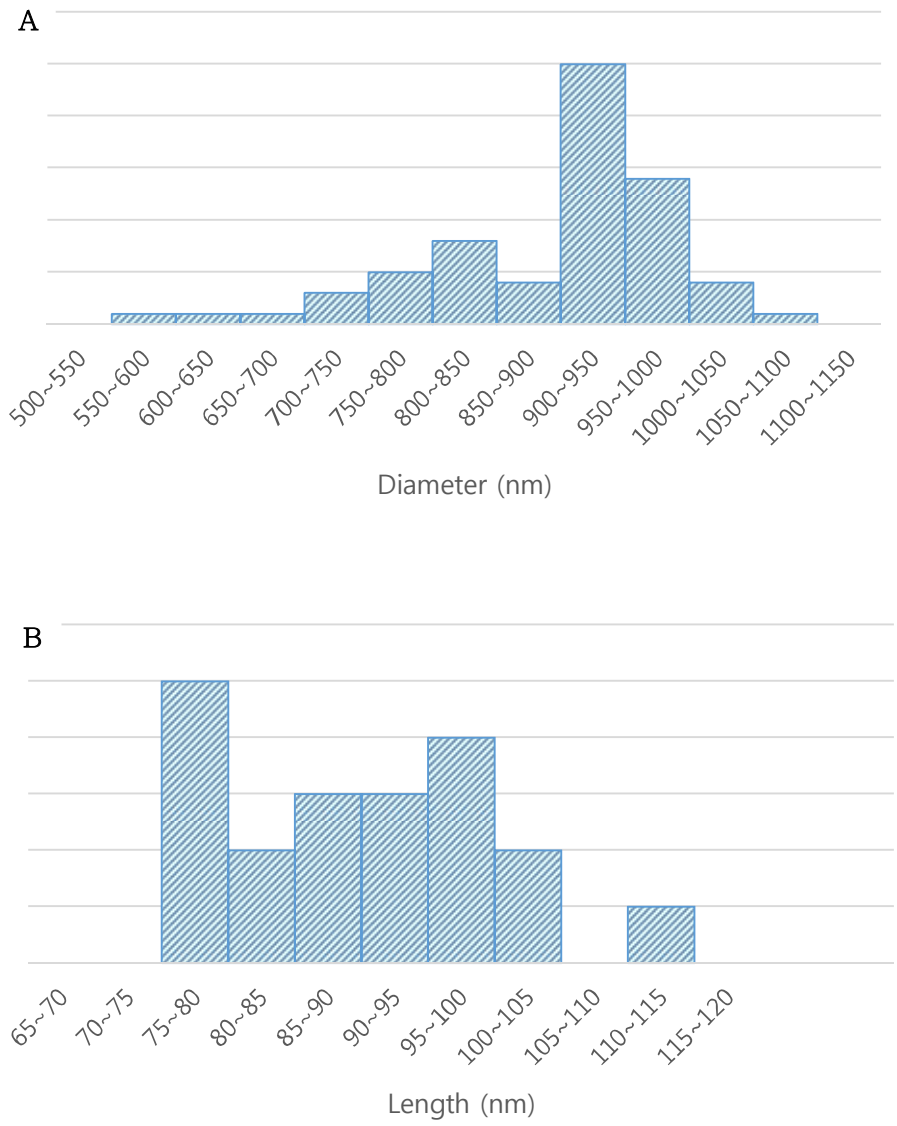

Figure 5 Size distribution histogram of HCS (A) and carbon shell thickness histogram of HCS (B)

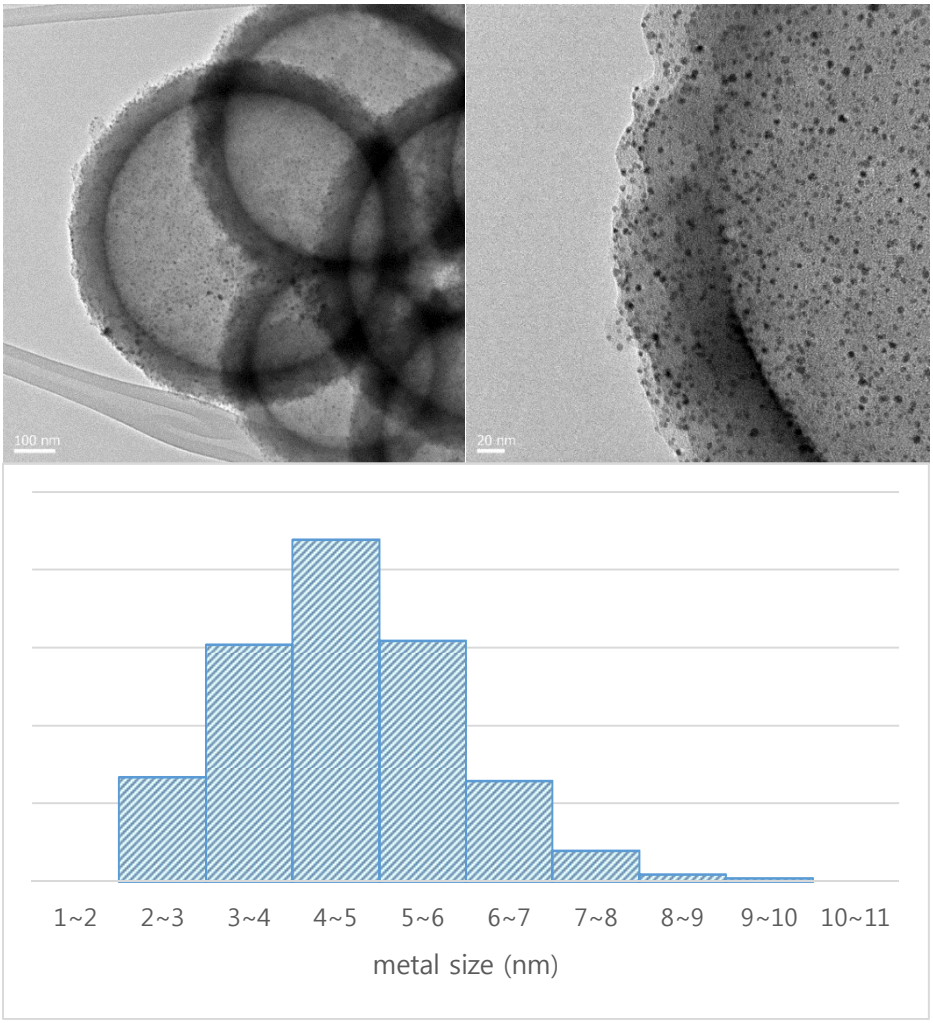

Figure 6 TEM images of $\boldsymbol{Pd_{(S)}/HCS_{(450)}}$ (A, B) and histogram of metal size distribution (C)

A B

C

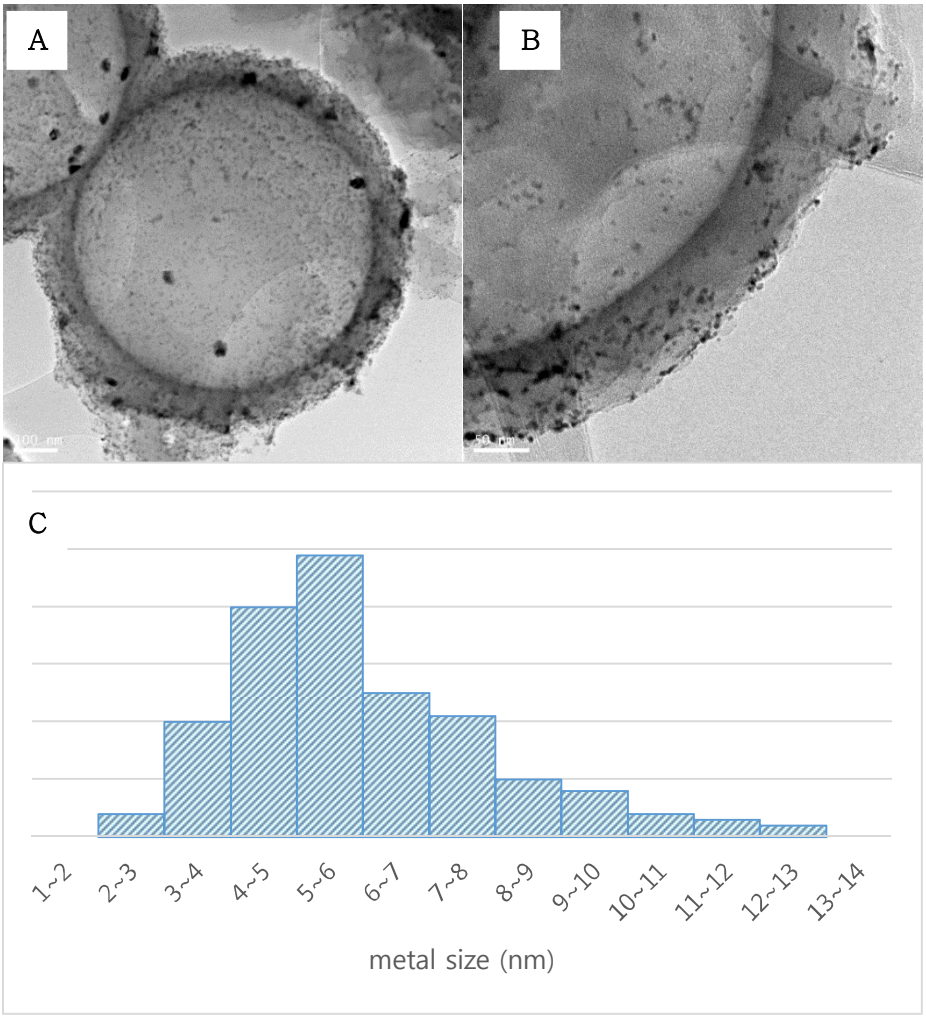

Figure 7 TEM images of $\boldsymbol{Pd-In_{(S)}/HCS_{(120)}}$ (A, B) and histogram of metal size distribution (C)

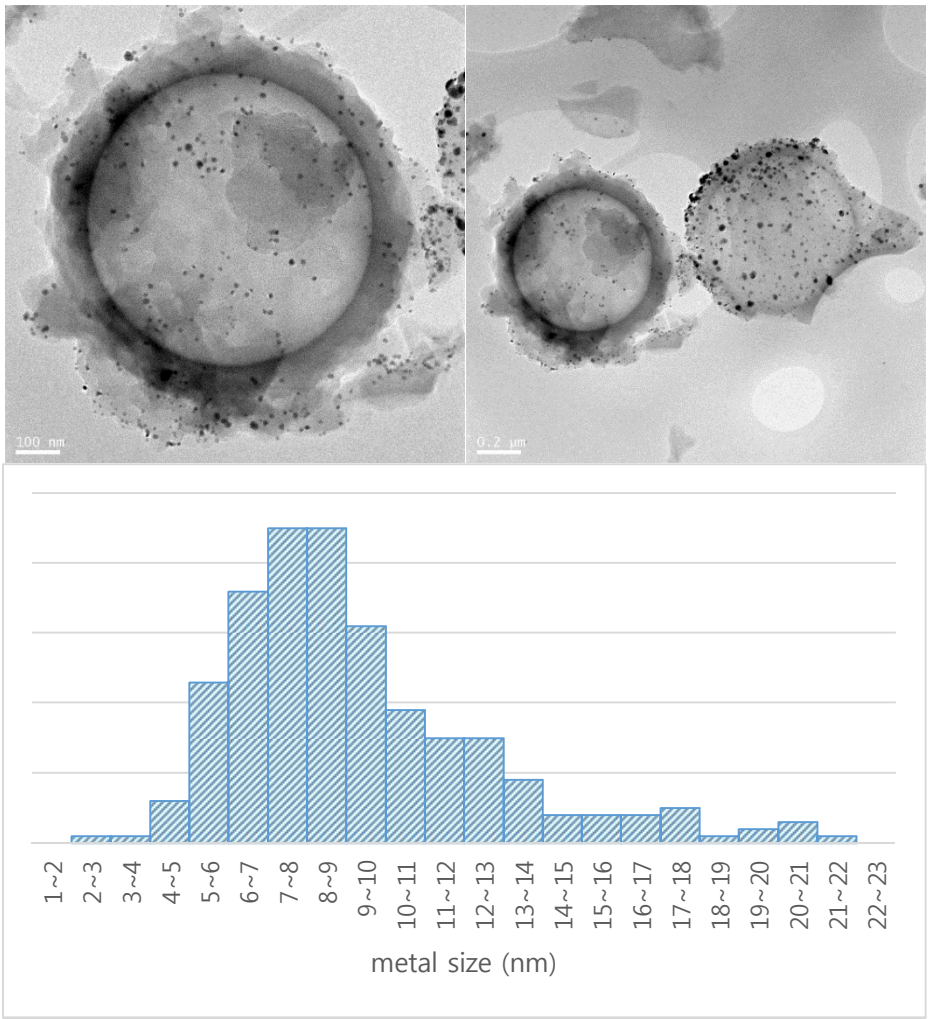

Figure 8 TEM images of $\boldsymbol{Pd-In_{(S)}/HCS_{(450)}}$ (A, B) and histogram of metal size distribution (C)

A B

C

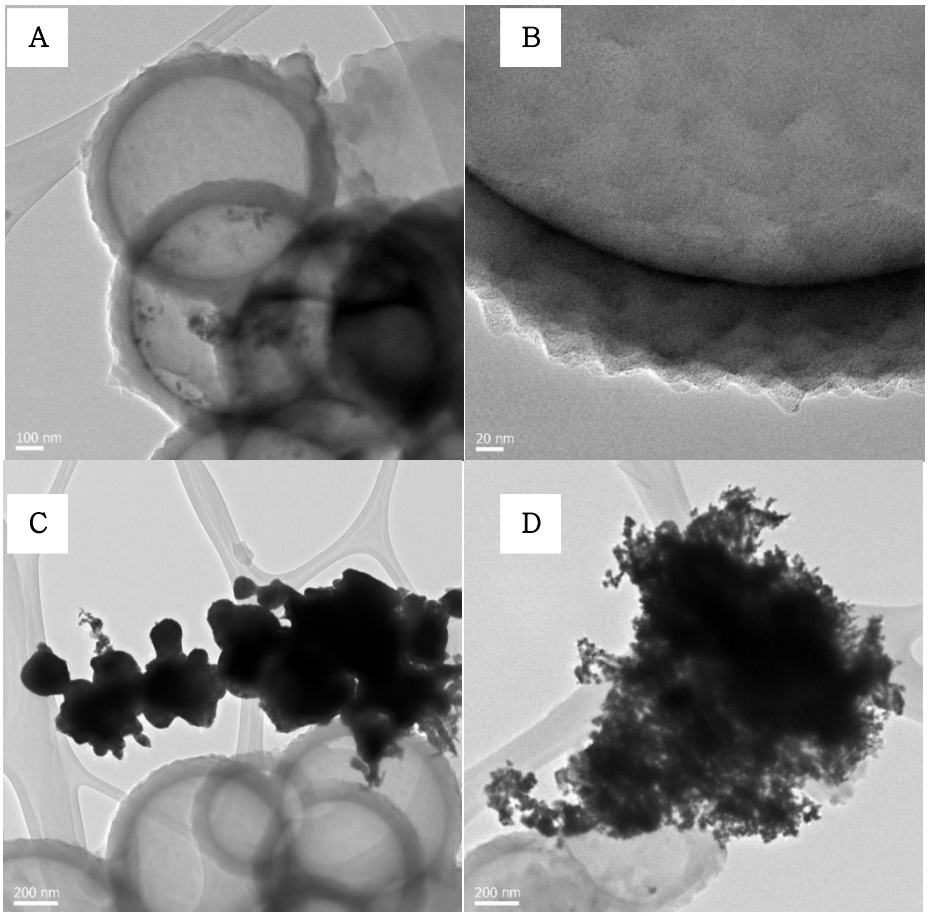

Figure 9 TEM images of $\boldsymbol{Pd-In_{(C)}/HCS_{(120)}}$ (A, B) and aggregation of metal (C, D)

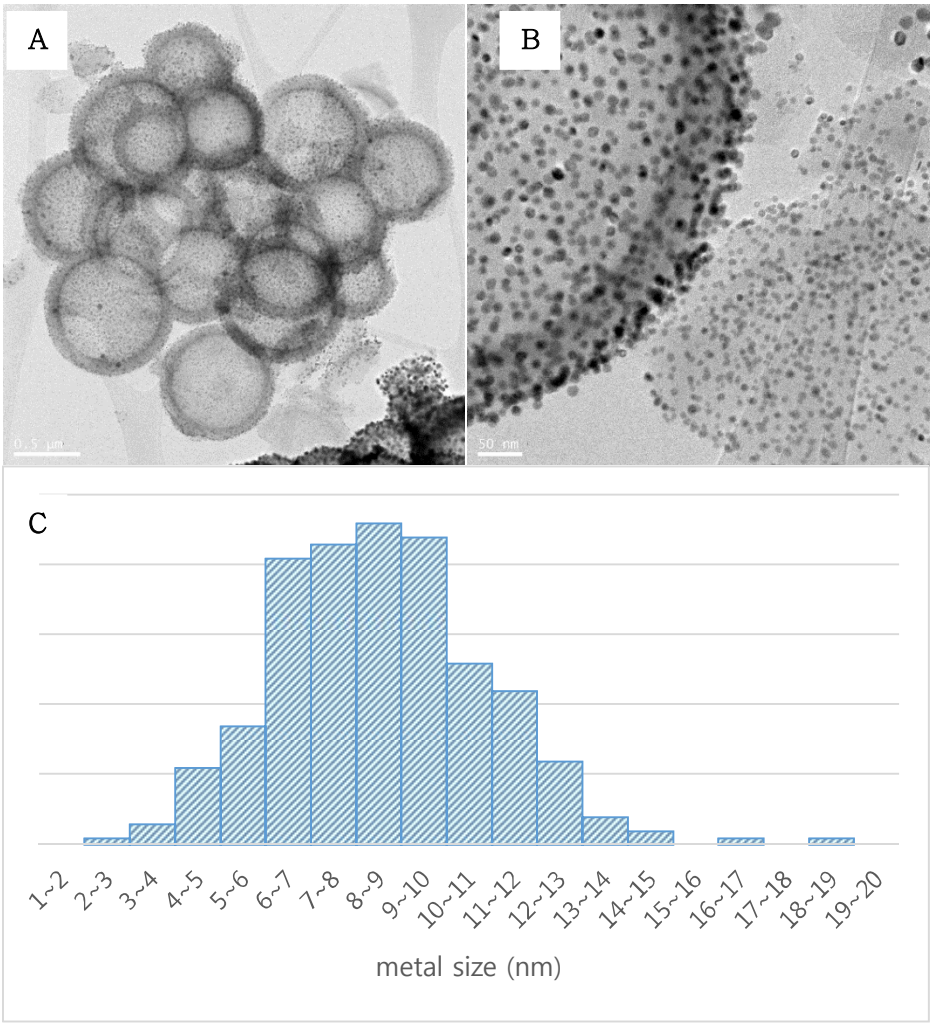

Figure 10 TEM images of $\boldsymbol{Pd-In_{(C)}/HCS_{(450)}}$ (A, B) and histogram of metal size distribution (C)

3.1.2 XRD Results

In order to determine crystalline structure of the catalysts, XRD characterization was carried out and the results were shown in Figure 11. The peaks at 40°, 46.7°, and 68° are characteristics of Pd(111), Pd(200), and Pd(220). At $Pd_{(S)}/HCS_{(450)}$ catalyst (Figure 11A), the observed characteristic of Pd was obviously presented. However, the In peaks were not observed at $Pd-In_{(S)}/HCS_{(120)}$ (Figure 11B) which could be explained by that none of In is metallized while preparing it or due to its relatively small amount of In used or lack of isolated indium nanoparticles on the surface of the support material. While Indium metal was not detected in the $Pd-In_{(S)}/HCS_{(120)}$ catalyst, it was detected in the $Pd-In_{(S)}/HCS_{(450)}$ catalyst in the form of alloy together with palladium. The peaks at 39.2°, 44.4°, 64.8°, and 78.5° are characteristics of $InPd_3$(111), $InPd_3$(200), $InPd_3$(220), and $InPd_3$(311), respectively. One of the possible explanation for this phenomenon is that the melting point of indium is 156.6℃

and the alloy was formed with Pd under the condition of reducing at 450℃ (Figure 11C). Unlike the metal salts used for the precursor, calcination and reducing temperature under 120℃ seems not sufficient enough for the removal of the acetate bonding between metals. However, when calcination and reducing temperature is raised up to 450℃, all of the remaining acetate is removed and pure InPd alloy is formed as shown in Figure 11D and E.

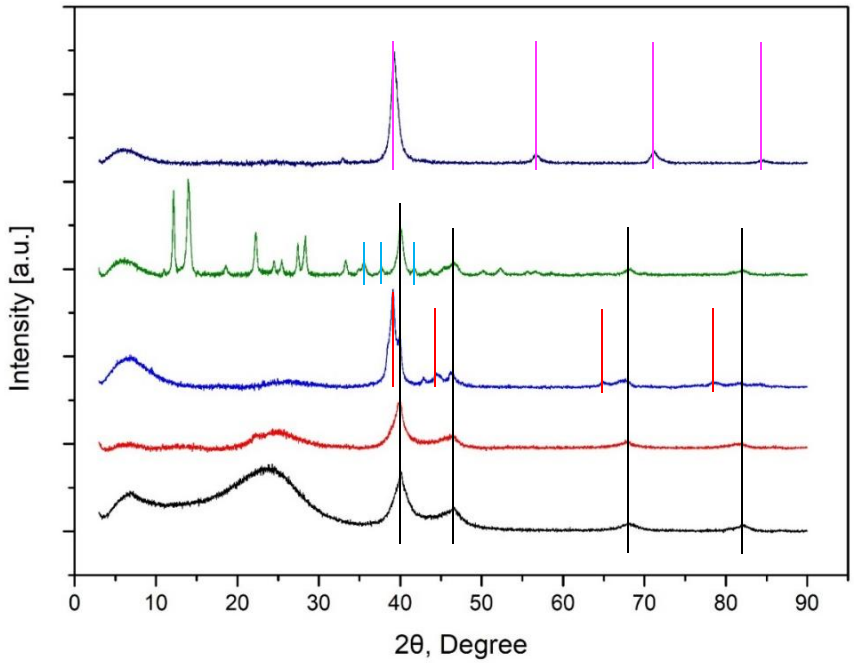

Figure 11 XRD patterns of $\boldsymbol{Pd_{(S)}/HCS_{(450)}}$ (A), $\boldsymbol{Pd-In_{(S)}/HCS_{(120)}}$ (B), $\boldsymbol{Pd-In_{(S)}/HCS_{(450)}}$ (C), $\boldsymbol{Pd-In_{(C)}/HCS_{(120)}}$ (D), $\boldsymbol{Pd-In_{(C)}/HCS_{(450)}}$ (E)
●: $\boldsymbol{InPd}$, ○: $\boldsymbol{InPd_3}$, ■: $\boldsymbol{Pd}$, △: $\boldsymbol{In_2O_3}$

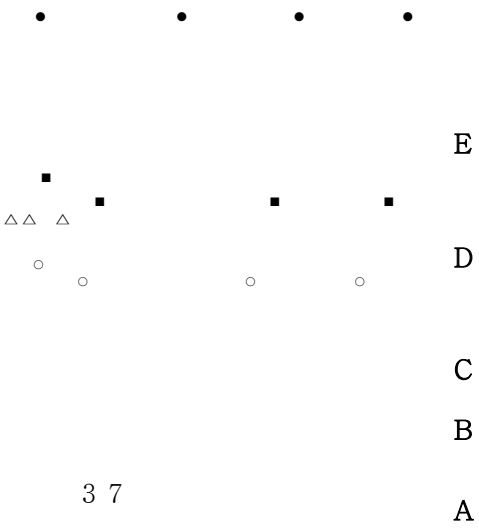

3.1.3 XPS Results

XPS was used to identify the valence of metals on the catalysts surface and the results are shown in Figure 12. The pair of peaks at 335.1 and 340.6eV is the characteristic of Pd(0) which is in accordance with previous studies. However, the peaks in the other catalysts except the catalyst shown in Figure 12C did not coincide with the above values, which is mainly shifted to the right. These peaks shifted to the right, thus, may be the Pd oxide. Similarly with Pd, XPS results on In metal were shown in Figure 13. The pair of peaks at 443.9 and 451.4eV represents the characteristic of In(0). Unlike the XPS result from Pd, In related peaks were not shown in all catalysts. This result suggests that all of the In that is deposited on the support is not in metallic state. Although the catalysts were treated in high temperature to reduce the metal, it is readily oxidized at the moment of contact with air. A very small size of metal may have affected these results as well.

3.1.4 ICP-OES Results

ICP-OES analysis was carried out to confirm the exact content of metals in each catalyst. The results for each catalyst are summarized in the fugure 14. $Pd_{(S)}/HCS_{(450)}$, $Pd-In_{(S)}/HCS_{(120)}$, $Pd-In_{(S)}/HCS_{(450)}$, $Pd-In_{(C)}/HCS_{(120)}$, and $Pd-In_{(C)}/HCS_{(450)}$ catalysts were loaded with 91.5, 87.7, 75.2, 76, and 103.1% of the desired Pd content, and, 0, 90.9, 64.7, 107.6, and 103.8% of the desired In content, respectively. As shown in the ICP analysis results, the contents of Pd and In at $Pd-In_{(C)}/HCS_{(120)}$ and $Pd-In_{(C)}/HCS_{(450)}$ catalyst are 1 : 1 since Pd-In complex has a unique structure of Pd and In which are connected to each other by acetate.

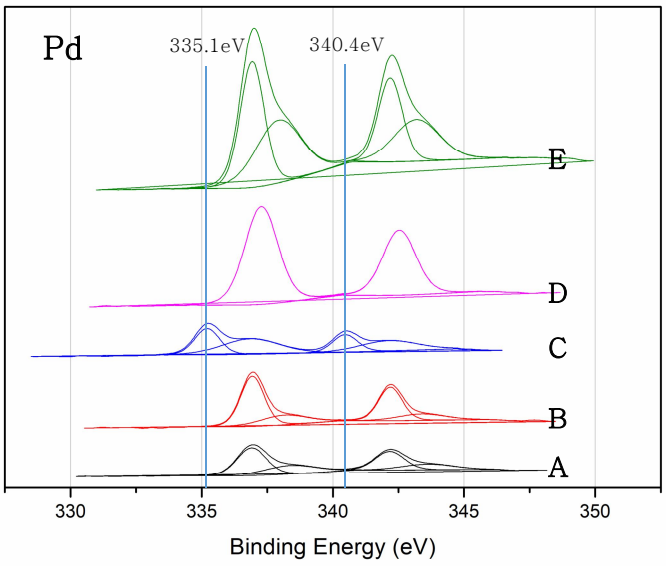

Figure 12 XPS spectrum of Pd for $\boldsymbol{Pd-In_{(S)}/HCS_{(120)}}$ (A), $\boldsymbol{Pd-In_{(S)}/HCS_{(450)}}$ (B), $\boldsymbol{Pd-In_{(C)}/HCS_{(120)}}$ (C), $\boldsymbol{Pd-In_{(C)}/HCS_{(450)}}$ (D), $\boldsymbol{Pd_{(S)}/HCS_{(450)}}$ (E) catalysts before reaction. 335.1 and 340.4 eV represents the $\boldsymbol{Pd^0}$ binding energy

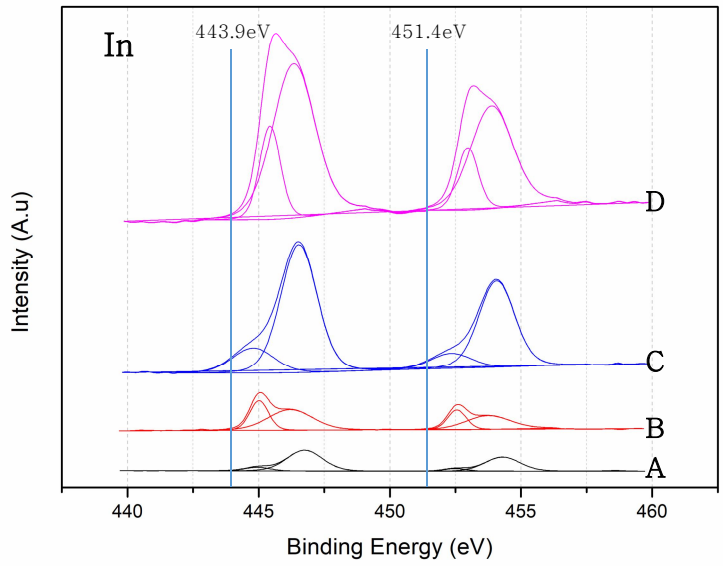

Figure 13 XPS spectrum of In for $\boldsymbol{Pd-In_{(S)}/HCS_{(120)}}$ (A), $\boldsymbol{Pd-In_{(S)}/HCS_{(450)}}$ (B), $\boldsymbol{Pd-In_{(C)}/HCS_{(120)}}$ (C), $\boldsymbol{Pd-In_{(C)}/HCS_{(450)}}$ (D) catalysts before the reaction. 443.9 and 451.4 eV represents the $\boldsymbol{In^0}$ binding energy

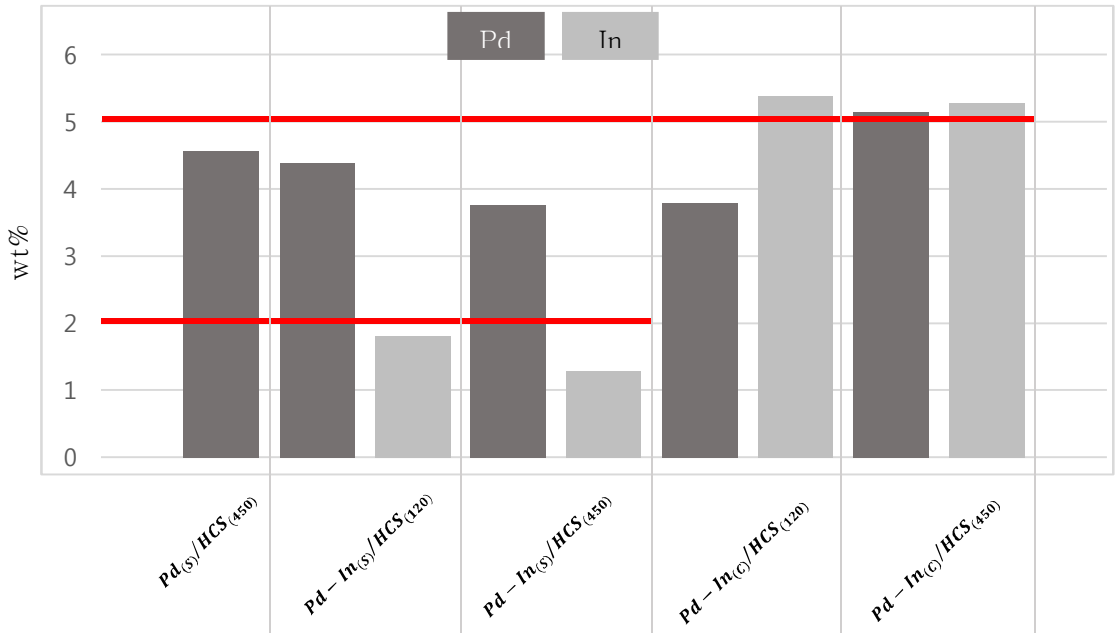

Figure 14 ICP-OES result of actual Pd and In content deposited on the HCS surface

3.2 Adsorptive Removal of Nitrate & Nitrite

To investigate the ability of HCS support, adsorption of nitrate and nitrite was investigated for the first time in this study. The initial concentration of nitrate and nitrite was set to 1 mM and detection of anions were performed after introducing 15 mM stock solution of $NaNO_2$ and $NaNO_3$ by sampling out 1 mL of aqueous solution every 30, 60, 120, and 180 minutes. Only small amount of both nitrate and nitrite was decreased. This meant that the adsorption of each anions rarely occurs in the citric-citrate buffer solution. Therefore, the adsorption removal of nitrate and nitrite was not considered in the following catalytic removal of nitrate and nitrite experiments.

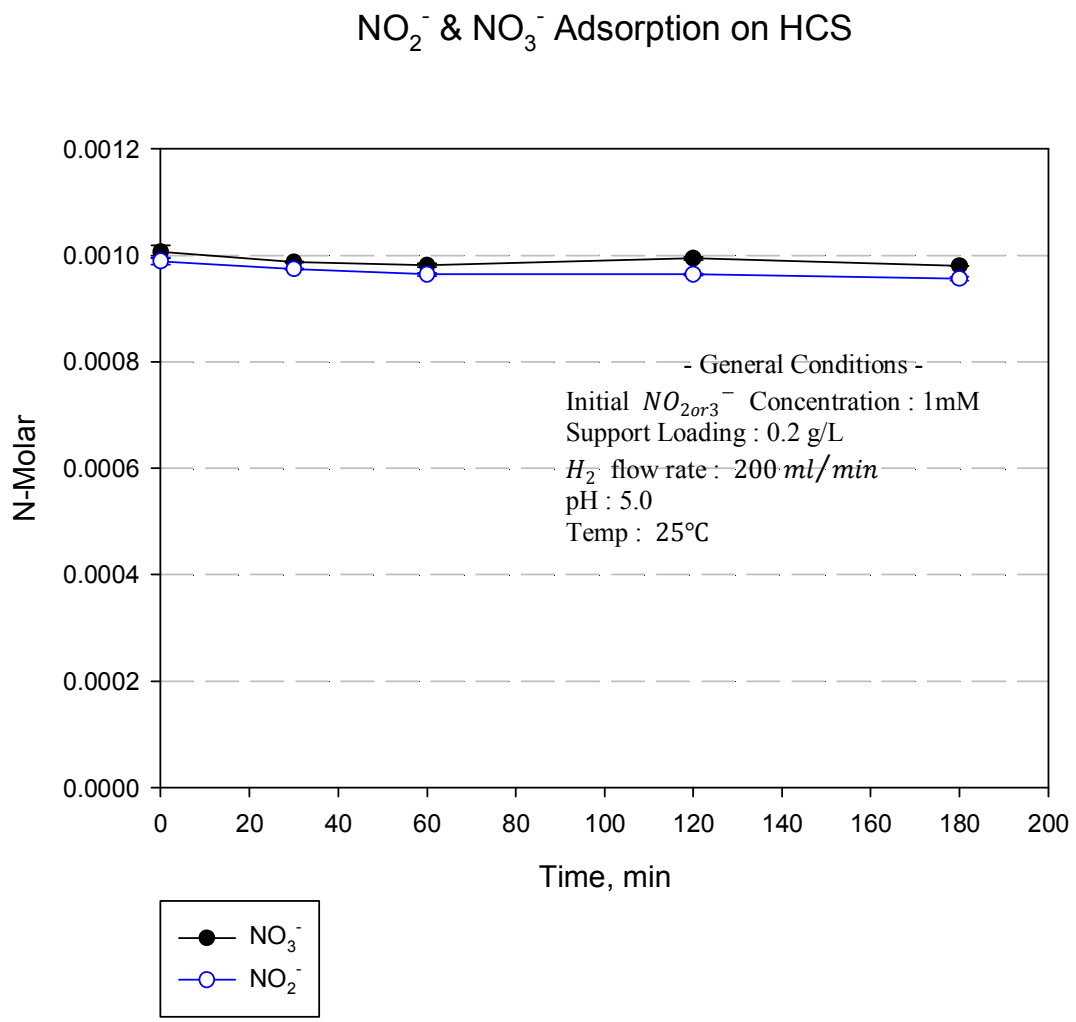

Figure 15 Nitrate and nitrite adsorption capability of HCS under citric-citrate buffer solution and hydrogen gas

3.3 Catalytic Removal of Nitrite

Although the founding from XPS result as described earlier that the charge of Pd was not zero state except $\mathrm{Pd-In}_{(C)}/HCS_{(120)}$ catalyst, all catalysts prepared in this study were active against nitrite reduction. Previous studies have shown that Pd should be in metallic state to reduce nitrite to nitrogen gas or ammonium before use. However, in the other previous studies[56], it was confirmed that $H_{2(g)}$ pretreatment at 25℃ reduces Ru/Al_2O_3 by reducing crystalline Ru oxide, in which the surface is oxidized upon the exposure to air, to metallic Ru from H_2-TPR analysis. Similar H_2-TPR result was also appeared in the other study of Pd/Al_2O_3 catalyst.[57] In this study, the Pd was not zero state as in the result of XPS, however it is expected to change to metallic Pd when $H_{2(g)}$ treatment is performed at room temperature for 30 min before use to reduce nitrite due to the redox-labile form of Pd.

Results from catalytic removal of nitrite are shown in Figure 14. Pd deposited alone on the HCS support

($\mathrm{Pd}_{(S)}/HCS_{(450)}$) showed highest nitrite reduction along with neligible formation of ammonia (<1%). However, the rate of nitrite removal and the selectivity to ammonia became different when In was introduced. Comparing $\mathrm{Pd}_{(S)}/HCS_{(450)}$ with $\mathrm{Pd-In}_{(S)}/HCS_{(120,450)}$ and $\mathrm{Pd-In}_{(C)}/HCS_{(120,450)}$, the latter two catalysts showed more than 2/3 of catalytic activity reduction and almost 25 times higher ammonia selectivity. What was unique was that nitrite removal rates did not differ significantly depending on which the metal precursor was used. On the other hand, there was a difference in the rate of nitrite reduction depending on the reduction temperature of the catalysts. The higher the temperature of the reduction of catalyst, the higher the reduction rate of nitrite. These results are due to the reduction state of Pd and distribution of Pd metal since nitrite removal occurs only on the Pd metal. The reason why the reduction of nitrite is slowed could be explained by the existence of In which blocks the active Pd metal sites.

If the amount of In is higher, it should block the active site of Pd metal as described earlier. The nitrite removal rate,

therefore, should be slower than the catalyst that has lower amount of In. The result of nitrite reduction from $\mathrm{Pd-In}_{(C)}/HCS_{(120,450)}$ catalyst showed slightly different ammonia yield result. Although there were higher amount of In in $\mathrm{Pd-In}_{(C)}/HCS_{(120,450)}$, ammonia formation was almost same or lower than in $\mathrm{Pd-In}_{(S)}/HCS_{(120,450)}$. This could be attributed to the unique structure of Pd–In complex in which In is directly next to Pd.

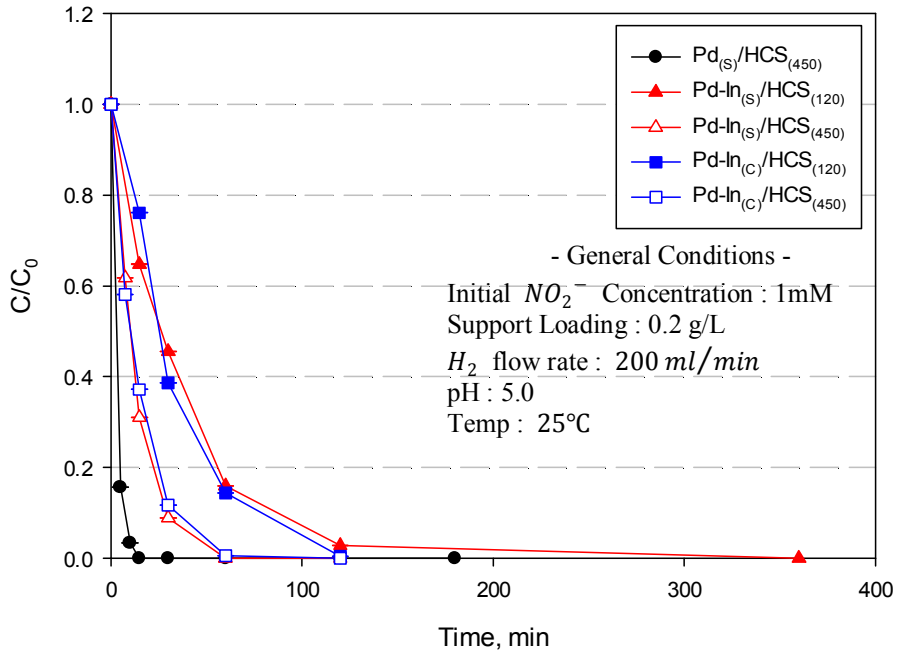

Figure 16 Catalytic reduction of nitrite

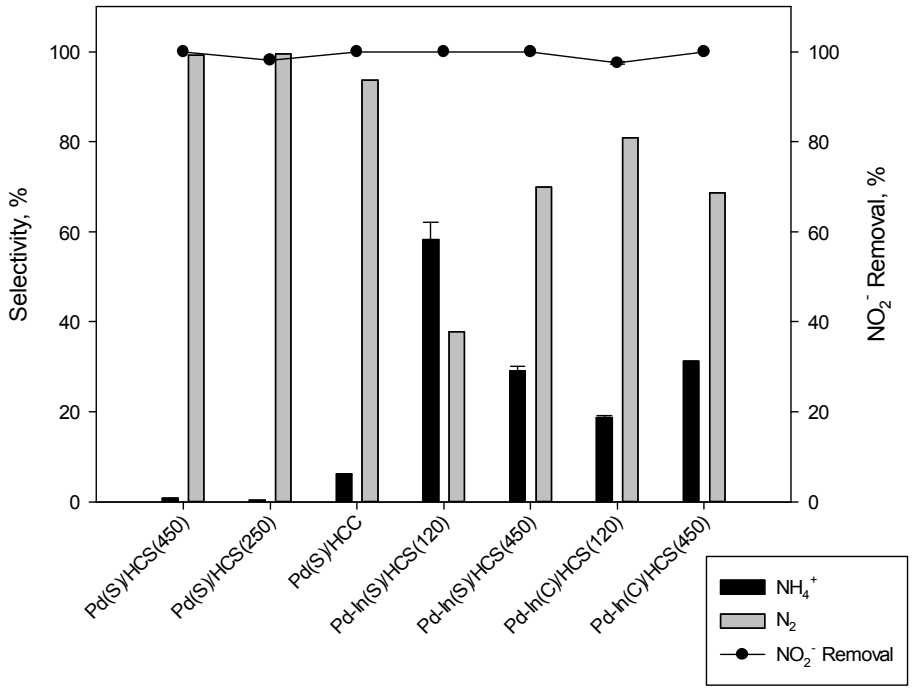

Figure 17 By-product selectivity and nitrite removal by different catalysts

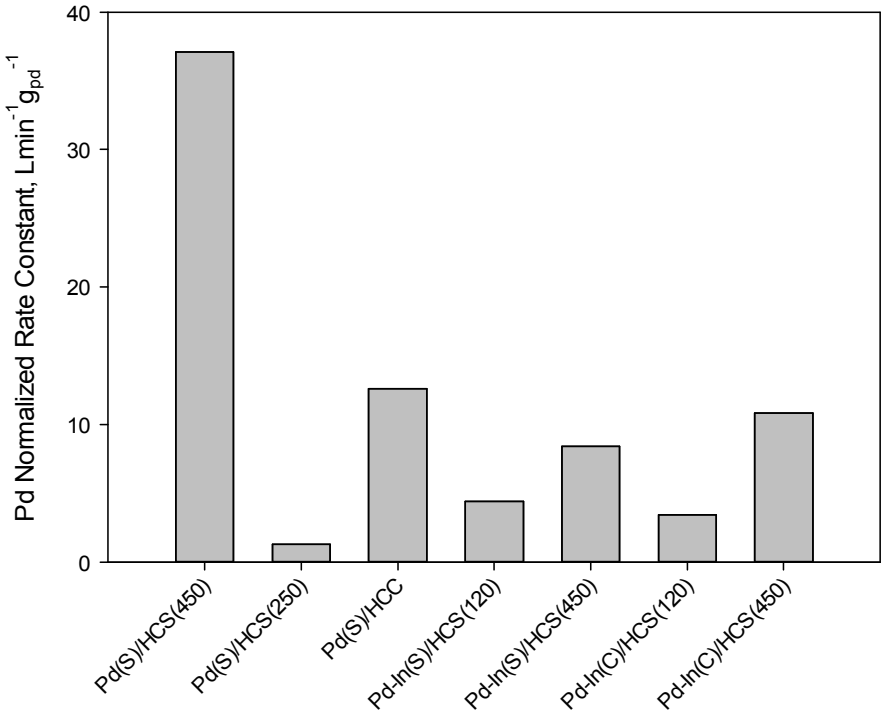

Figure 18 Catalytic nitrite reduction kinetics

3.4 Catalytic Removal of Nitrate

Figure 17 shows the catalytic reduction of nitrate by $\mathrm{Pd-In}_{(S)}/HCS_{(120)}$, $\mathrm{Pd-In}_{(S)}/HCS_{(450)}$, $\mathrm{Pd-In}_{(C)}/HCS_{(120)}$, and $\mathrm{Pd-In}_{(C)}/HCS_{(450)}$. It was confirmed that there was no metallic Pd and In phases on the catalysts surface via XPS analysis(Figure 12), except the zero state of Pd metal from $\mathrm{Pd-In}_{(C)}/HCS_{(120)}$. Although the results from XPS showed that In was not metallic In, about 93% of the nitrate was removed from $Pd-In_{(S)}/HCS_{(450)}$ catalyst and the kinetic was highest among the catalysts tested for nitrate removal in this study. From section 3.2, it was evidenced that adsorptive removal of nitrate does not occurs. Thus, it can be concluded that nitrate was reduced by the catalyst reaction using hydrogen as an electron donor. Except $Pd-In_{(S)}/HCS_{(450)}$ catalyst, all other catalysts showed very low or negligible amount of nitrate was removed. Although we could not observed the reduction results over a long period of time for $Pd-In_{(S)}/HCS_{(120)}$ and $Pd-In_{(C)}/HCS_{(450)}$ catalyst, $Pd-In_{(S)}/HCS_{(450)}$ catalyst showed very high

nitrate reduction among the catalysts, from the results of nitrate reduction up to 360 min, it is believed that the reduction temperature of catalyst contributed to the ammonia formation in both using Pd-In salt and Pd-In complex as metal precursor shown in Figure 20. In addition, it can be concluded that ammonia generation was lower when the Pd-In Complex material was used regardless of the reduction temperature of the catalyst. This seems to be the result of the many In atoms located adjacent to the Pd.

From the result of TEM images which showed very uniform size and wide distribution of metal nanoparticles and nitrate reduction experiment which generated less amount of ammonia when Pd-In complex is used as the metal precursor, it is highly expected to obtain improved nitrate removal and low production of ammonia as by-product if we can reliably make metal oxidation state to zero.

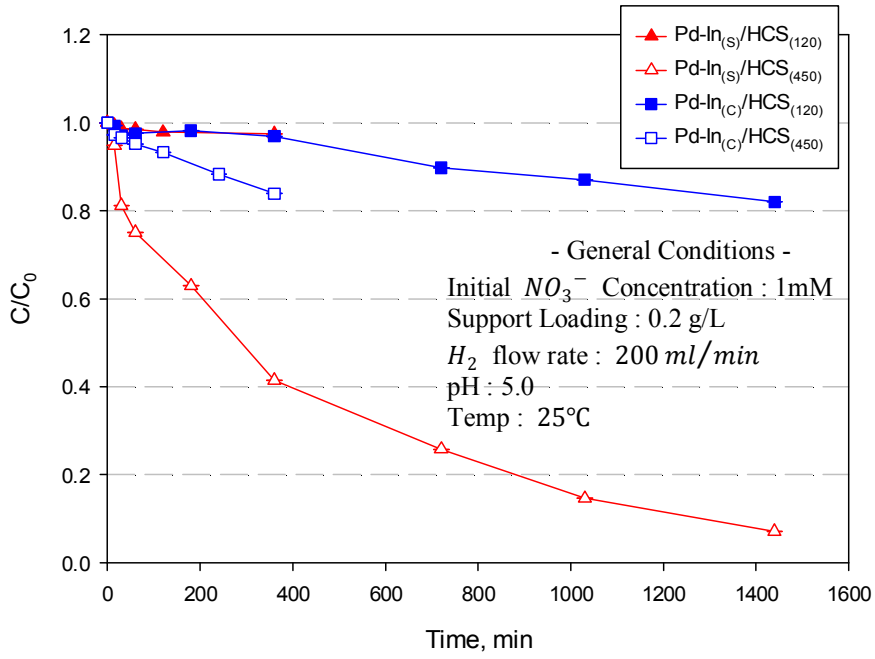

Figure 19 Catalytic reduction of nitrate

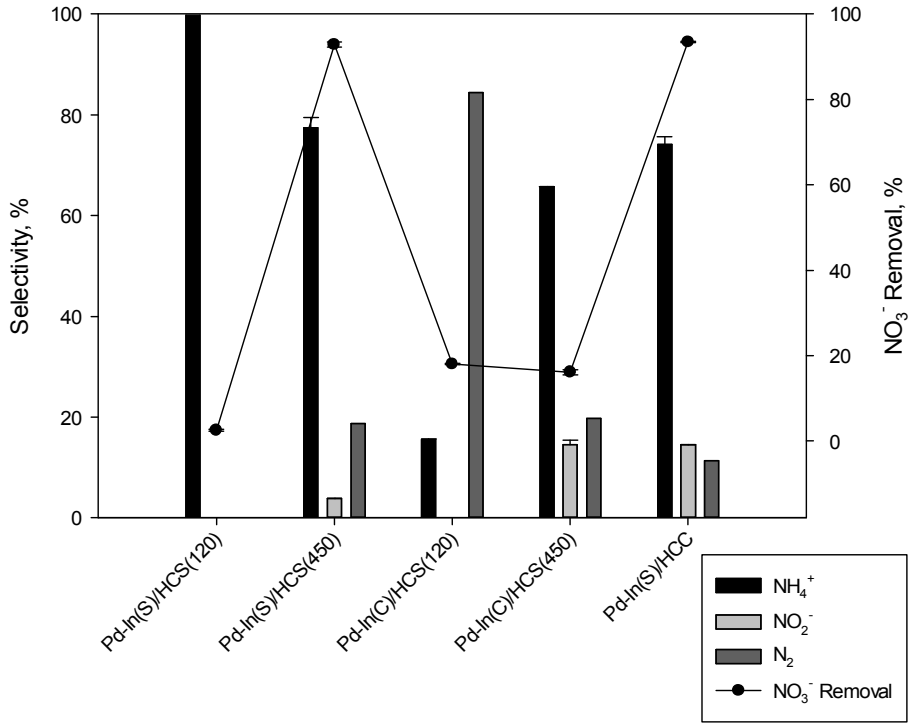

Figure 20 By-product selectivity and nitrate removal by different catalysts

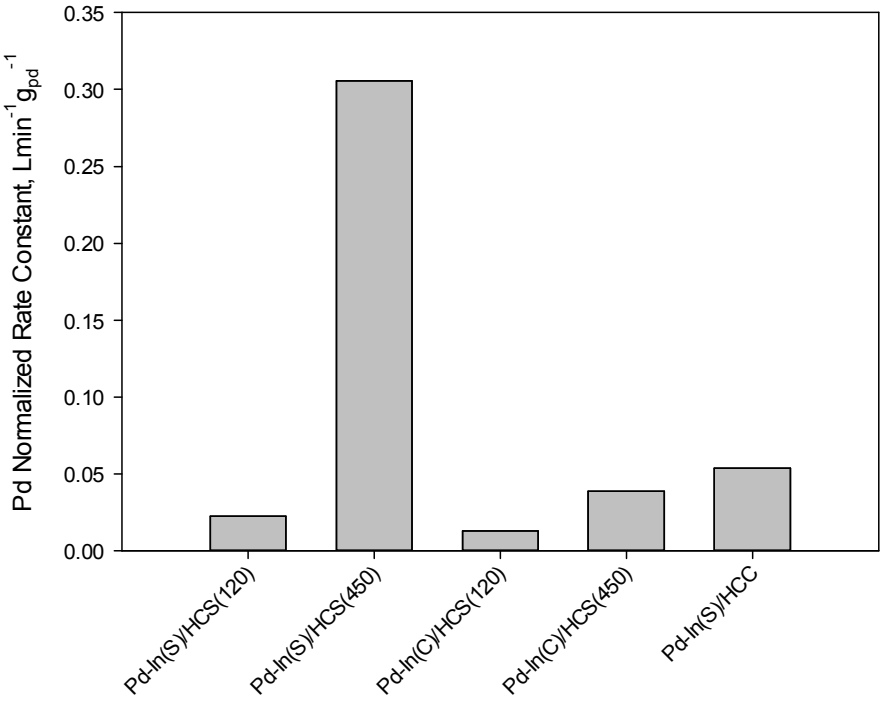

Figure 21 Catalytic nitrate reduction kinetics

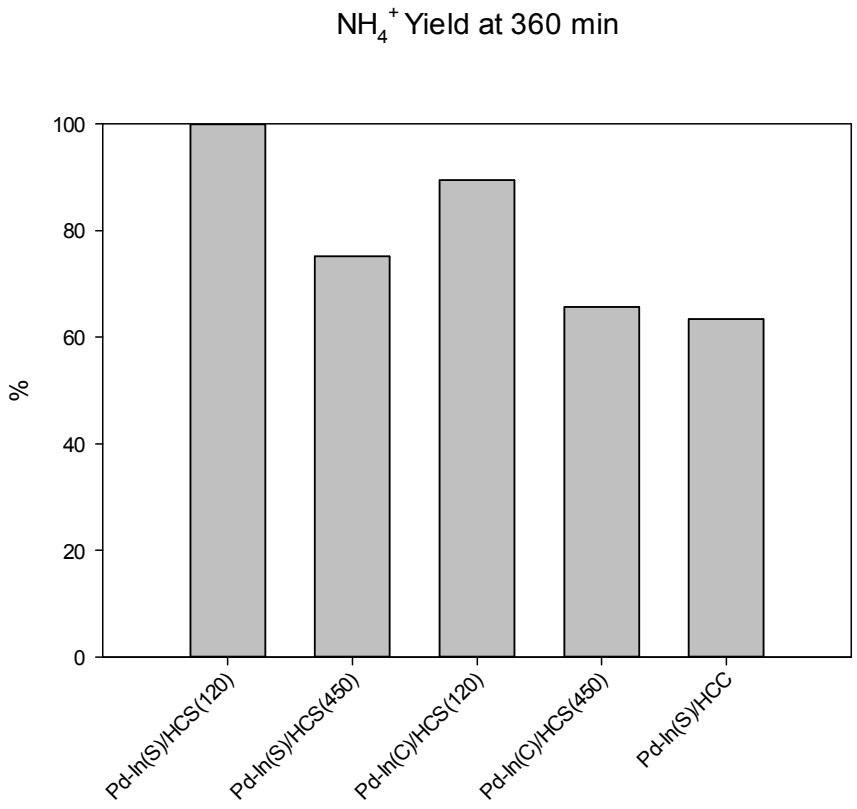

Figure 22 By-product selectivity of nitrate reduction by different catalysts at 360 min

Chapter 4. Conclusion

Pd-In bimetallic catalyst was synthesized using hollow carbon sphere to reduce nitrate and nitrite to nitrogen gas. TEM images showed that HCS was formed well through carbonization of PS/PANi core-shell polymer and confirmed the very high distribution of Pd and In nanoparticles on HCS surface under the proposed catalyst preparation condition. XRD analysis confirmed that crystalline structure of Pd was observed from $Pd_{(S)}/HCS_{(450)}$ catalyst and crystalline structure of In_1Pd_1 from $Pd-In_{(C)}/HCS_{(450)}$ catalyst. Besides, reduction temperature of 450℃ is required to obtain high quality of $\mathrm{Pd-In/HCS}$ catalyst when Pd-In Complex is used for the metal precursor. $Pd_{(S)}/HCS_{(450)}$ catalyst showed fastest removal (< 15 min) in nitrite reduction than in any other Pd catalysts, however the presence of In in nitrite removal seemed to affect the ammonia formation rather than Pd catalysts. Our results showed that nitrate and nitrite can be reduced even when Pd and In are not in metallic state. Pd and In leaching was not

detected during two reaction cycles. The reaction mechanism of catalytic nitrate reduction by Pd-In/HCS verified by nitrate and nitrite reduction experiments can be explained by two-steps;

(1) reduction of nitrate to nitrite coupled with oxidation of In

(2) nitrite is subsequently reduced to nitrogen gas or ammonium by hydrogen molecules adsorbed on the adjacent active sites of Pd.

Reference

1. Wakida, F. T. & Lerner, D. N. Non-agricultural sources of groundwater nitrate: A review and case study. *Water Res.* **39**, 3–16 (2005).
2. Spalding, R. F. & Exner, M. E. (1993) Occurrence of Nitrate in Groundwater-A Review. *Water* **22**, 392–402 (1993).
3. Weyer, P. J. *et al.* Municipal drinking water nitrate level and cancer risk in older women: The Iowa women's health study. *Epidemiology* **12**, 327–338 (2001).
4. Gulis, G., Czompolyova, M. & Cerhan, J. R. An ecologic study of nitrate in municipal drinking water and cancer incidence in Trnava District, Slovakia. *Environ. Res.* **88**, 182–187 (2002).
5. Rogan, W. J. & Brady, M. T. Drinking Water From Private Wells and Risks to Children. *Pediatrics* **123**, e1123–e1137 (2009).
6. Environmental Protection Agency. *Fed. Regist.* **62**, 1811–1844 (2002).
7. Choe, J. K. *et al.* Performance and life cycle environmental benefits of recycling spent ion exchange brines by catalytic treatment of nitrate. *Water Res.* **80**, 267–280 (2015).
8. Samatya, S., Kabay, N., Yüksel, Ü., Arda, M. & Yüksel, M. Removal of nitrate from aqueous solution by nitrate selective ion exchange resins. *React. Funct. Polym.* **66**, 1206–1214 (2006).
9. Schoeman, J. J. & Steyn, A. Nitrate removal with reverse osmosis in a rural area in South Africa. *Desalination* **155**, 15–26 (2003).
10. El Midaoui, A. *et al.* Optimization of nitrate removal operation from ground water by electrodialysis. *Sep. Purif. Technol.* **29**, 235–244 (2002).
11. Park, J. Y. & Yoo, Y. J. Biological nitrate removal in industrial wastewater treatment: Which electron donor we can choose. *Appl. Microbiol. Biotechnol.* **82**, 415–429 (2009).

12. Bhatnagar, A. & Sillanpää, M. A review of emerging adsorbents for nitrate removal from water. *Chem. Eng. J.* **168**, 493–504 (2011).
13. Kapoor, A.; V. & T. Nitrate removal from drinking water. *J. Environ. Eng. 1997* **123**, 371–380 (1997).
14. Hell, F., Lahnsteiner, J., Frischherz, H. & Baumgartner, G. Experience with full-scale electrodialysis for nitrate and hardness removal. *Desalination* **117**, 173–180 (1998).
15. Shrimali, M. & Singh, K. P. New methods of nitrate removal from water. *Environ. Pollut.* **112**, 351–359 (2001).
16. Mikami, I., Yoshinaga, Y. & Okuhara, T. Rapid removal of nitrate in water by hydrogenation to ammonia with Zr-modified porous Ni catalysts. *Appl. Catal. B Environ.* **49**, 173–179 (2004).
17. Gao, W. *et al.* Titania supported Pd-Cu bimetallic catalyst for the reduction of nitrate in drinking water. *Appl. Catal. B Environ.* **46**, 341–351 (2003).
18. Chen, Y. X., Zhang, Y. & Chen, G. H. Appropriate conditions or maximizing catalytic reduction efficiency of nitrate into nitrogen gas in groundwater. *Water Res.* **37**, 2489–2495 (2003).
19. Xie, Y., Cao, H., Li, Y., Zhang, Y. & Crittenden, J. C. Highly selective PdCu/amorphous silica-alumina (ASA) catalysts for groundwater denitration. *Environ. Sci. Technol.* **45**, 4066–4072 (2011).
20. Matatov-Meytal, Y. *et al.* Cloth catalysts for water denitrification. *Appl. Catal. B Environ.* **31**, 233–240 (2002).
21. Hôrold, S., Tacke, T. & Vorlop, K. D. Catalytical removal of nitrate and nitrite from drinking water: 1. screening for hydrogenation catalysts and influence of reaction conditions on activity and selectivity. *Environ. Technol. (United Kingdom)* **14**, 931–939 (1993).
22. Hörold, S., Vorlop, K. D., Tacke, T. & Sell, M. Development of catalysts for a selective nitrate and nitrite removal from drinking water. *Catal. Today* **17**, 21–30 (1993).
23. Soares, O. S. G. P., Órfão, J. J. M. & Pereira, M. F. R.

Bimetallic catalysts supported on activated carbon for the nitrate reduction in water: Optimization of catalysts composition. *Appl. Catal. B Environ.* **91**, 441–448 (2009).
24. Epron, F., Gauthard, F. & Barbier, J. Catalytic reduction of nitrate in water on a monometallic Pd/CeO2 catalyst. *J. Catal.* **206**, 363–367 (2002).
25. Prüsse, U. & Vorlop, K. D. Supported bimetallic palladium catalysts for water-phase nitrate reduction. *J. Mol. Catal. A Chem.* **173**, 313–328 (2001).
26. Jung, J., Bae, S. & Lee, W. Nitrate reduction by maghemite supported Cu-Pd bimetallic catalyst. *Appl. Catal. B Environ.* **127**, 148–158 (2012).
27. Bae, S., Jung, J. & Lee, W. The effect of pH and zwitterionic buffers on catalytic nitrate reduction by TiO2-supported bimetallic catalyst. *Chem. Eng. J.* **232**, 327–337 (2013).
28. Liou, Y. H., Lin, C. J., Weng, S. C., Ou, H. H. & Lo, S. L. Selective decomposition of aqueous nitrate into nitrogen using iron deposited bimetals. *Environ. Sci. Technol.* **43**, 2482–2488 (2009).
29. Guy, K. A., Xu, H., Yang, J. C., Hurley, K. D. & Shapley, J. R. Catalytic nitrate and nitrite reduction with Pd-Cu colloids: Composition, structure and reactivity correlations. *231st ACS Natl. Meet.* ENVR-080 (2006).
30. Prüsse, U., Hähnlein, M., Daum, J. & Vorlop, K. D. Improving the catalytic nitrate reduction. *Catal. Today* **55**, 79–90 (2000).
31. Chaplin, B. P., Shapley, J. R. & Werth, C. J. The selectivity and sustainability of a Pd-In/γ-Al 2 O 3 catalyst in a packed-bed reactor: The effect of solution composition. *Catal. Letters* **130**, 56–62 (2009).
32. Chaplin, B. P., Shapley, J. R. & Werth, C. J. Regeneration of sulfur-fouled bimetallic Pd-based catalysts. *Environ. Sci. Technol.* **41**, 5491–5497 (2007).
33. Marchesini, F. A., Irusta, S., Querini, C. & Miró, E. Nitrate hydrogenation over Pt,In/Al2O3 and Pt,In/SiO2. Effect of aqueous media and catalyst surface properties upon the catalytic activity. *Catal. Commun.* **9**, 1021–1026 (2008).
34. Marchesini, F. A., Irusta, S., Querini, C. & Miró, E.

Spectroscopic and catalytic characterization of Pd−In and Pt−In supported on Al2O3 and SiO2, active catalysts for nitrate hydrogenation. *Appl. Catal. A Gen.* **348**, 60–70 (2008).
35. Gao, Z. *et al.* Highly active Pd−In/mesoporous alumina catalyst for nitrate reduction. *J. Hazard. Mater.* **286**, 425–431 (2015).
36. Lemaignen, L., Tong, C., Begon, V., Burch, R. & Chadwick, D. Catalytic denitrification of water with palladium−based catalysts supported on activated carbons. **75**, 43–48 (2002).
37. Bell, A. T. The Impact of Nanoscience on Heterogeneous Catalysis. **299**, 1688–1692 (2003).
38. Zaera, F. heterogeneous catalysis † is. **2**, 2746–2762 (2013).
39. Xu, Y., Chen, L., Wang, X., Zhang, Q. & Chen, L. nanocatalysts : colloidal synthesis , properties , and. 10559–10583 (2015). doi:10.1039/c5nr02216a
40. Guang−zhi, Y. *et al.* Hollow carbon nanospheres prepared by carbonizing polymethylmethacrylate / polyacrylonitrile core / shell polymer particles. *New Carbon Mater.* **23**, 205–208 (2008).
41. Ahiro, A. K. Preparation and Characteristics of Fine Hollow Carbon Particles. **328**, 325–328 (1996).
42. Yang, M. *et al.* Phenolic Resin and Derived Carbon Hollow Spheres. 1633–1639 (2006). doi:10.1002/macp.200600273
43. Pdvb, P. & Shell, C. Fabrication of Carbon Nanocapsules Using PMMA/PDVB Core/Shell Nanoparticles. *Chem. Mater.* **15**, 2002–2004 (2003).
44. Xiao−ying, D. A. I., Xin, Z., Yi−fei, M. & Pei−kang, S. Preparation of hollow carbon spheres by carbonization of polystyrene / polyaniline core−shell polymer particles. *New Carbon Mater.* **26**, 389–395 (2011).
45. Khan, M. A. & Armes, S. P. Synthesis and characterization of micrometer−sized poly(3,4−ethylenedioxythiophene)−coated polystyrene latexes. *Langmuir* **15**, 3469–3475 (1999).
46. Stolarov, I. P. *et al.* First platinum (ii)– alkaline−earth

acetate−bridged complexes Pt ii (m −OAc) 4 M ii (AcOH) 4 (M = Ca , Sr , Ba). *Mendeleev Commun.* **4**, 200–201 (2018).
47. Kozitsyna, N. Y. *et al.* Synthesis , crystal structure and thermal redox transformations of palladium (II)– alkaline earth tetraacetate−bridged lantern complexes Pd II (μ − OOCMe) 4 M II (HOOCMe) 4 (M = Ca , Sr , Ba). *Mendeleev Commun.* **569**, 261–263 (2007).
48. Ploeg, A. F. M. J. V. A. N. D. E. R., Koten, G. V. A. N. & Vrieze, K. Synthesis of Novel Binuclear Palladium−Thallium Carboxylates of the Type PdTl(O2CH)5, and their Structural Characterization Based on Observation of J(203,205Tl−H) and J(203,205Tl−C). *Inorganica Chim. Acta,* **39**, 253–261 (1980).
49. Balch, L., Davis, B. J. & Fung, E. Y. Palladium−thallium interactions in dinuclear complexes with structural components that place the two metal centers in close proximity. *Inorganza Chwruca Acta* **212**, 149–156 (1993).
50. Stolarov, I. P. *et al.* Heterometallic Palladium (II) − Indium (III) and − Gallium (III) Acetate− Bridged Complexes : Synthesis , Structure , and Catalytic Performance in Homogeneous Alkyne and Alkene Hydrogenation. *Inorg. Chem.* **57**, 11482–11491 (2018).
51. Zhang, R., Shuai, D., Guy, K. A. & Shapley, J. R. Elucidation of Nitrate Reduction Mechanisms on a Pd−In Bimetallic Catalyst using Isotope Labeled Nitrogen Species. 313–321 (2013). doi:10.1002/cctc.201200457
52. Salmit, T., Warnat, J. & Maunulas, T. Kinetics of nitrate reduction reactor. **0009**, 5763–5773 (1995).
53. Gurrath, M. *et al.* Palladium catalysts on activated carbon supports. *Carbon N. Y.* **38**, 1241–1255 (2002).
54. Dantas Ramos, A. L., da Silva Alves, P., Aranda, D. A. G. & Schmal, M. Characterization of carbon supported palladium catalysts: Inference of electronic and particle size effects using reaction probes. *Appl. Catal. A Gen.* **277**, 71–81 (2004).
55. Soares, O. S. G. P. *et al.* Pd−Cu/AC and Pt−Cu/AC catalysts for nitrate reduction with hydrogen: Influence of calcination and reduction temperatures. *Chem. Eng. J.* **165**,

78–88 (2010).
56. Huo, X., Van Hoomissen, D. J., Liu, J., Vyas, S. & Strathmann, T. J. Hydrogenation of aqueous nitrate and nitrite with ruthenium catalysts. *Appl. Catal. B Environ.* **211**, 188–198 (2017).
57. Vedyagin, A. A. *et al.* Characterization of active sites of Pd/Al2O3 model catalysts with low Pd content by luminescence, EPR and ethane hydrogenolysis. *Appl. Catal. B Environ.* **103**, 397–403 (2011).

Abstract in Korean

과도한 비료 사용으로 인해 질산염과 아질산염에 대한 지하수 및 지표수의 오염이 지속적으로 증가하고 있다. 이런 오염물질을 적절히 제거하거나 처리하지 않는다면 신생아청색증 (methemo-globinemia)나 암을 유발할 수 있다. 질산염과 아질산염의 이러한 유해성으로 인해 U.S.EPA에서는 질산염과 아질산염의 최대 농도를 각각 $10\,mg-N/L$ 및 $1\,mg-N/L$로 규제하고 있다. 촉매적 처리는 수소를 전자 공여체로 사용하여 질산염과 아질산염을 질소가스로 지속적으로 환원시킬 수 있어 유망한 기술로 떠오르고 있다. 하지만 지금까지의 질산염과 아질산염에 대한 촉매적 제거 연구는 부산물 중 하나인 암모니아의 발생으로 인해 한계가 있다. 본연구에서는 이러한 한계점을 극복하기 위해 Pd 기반 촉매를 hollow carbon sphere (HCS)에 담지한 Pd 및 Pd-In/HCS 촉매를 개발하였다. 본 촉매를 이용하여 아질산염을 환원하는 동안 매우 낮은 암모니아가 발생하는 것을 확인하였으며 (초기 아질산염 농도의 1% 이하), 아질산염 환원 또한 타 촉매에 비해 매우 높은 활성을 가지는 것을 확인하였다. 또한 질산염을 환원하는 실험을 진행하였으며 본 촉매의 물리적 화학적 특성을 파악하기 위해 투과 전자 현미경 (TEM), X선 회절 (XRD), X선 광전자분광 (XPS)을

이용하여 촉매의 형태, 금속의 분산 정도, 결정구조, 금속의 화학적 산화상태를 분석하였다. 질산염과 아질산염이 질소가스나 암모니아로 환원되는 반응경로에서 귀금속과 HCS의 역할에 대해 귀금속의 결정구조와 산화상태, 질산염과 아질산염에 대한 HCS의 흡착 가능성을 평가함으로써 조사하였다. 본 연구의 결과는 질산염과 아질산염을 처리하는 동안 Pd-In/HCS 촉매의 선택성과 반응성을 향상시키기 위한 광범위한 의미와 적용 가능성을 갖는다.